Giant Negative Linear Compressibility in Orthorhombic Copper Cyanide

Swayam Kesari,[1] Alka B. Garg,[2,3] Nilesh P. Salke,[1,4,*] and Rekha Rao[1,3,†]
[1]Solid State Physics Division, Bhabha Atomic Research Centre, Mumbai 400085, India
[2]High Pressure and Synchrotron Radiation Physics Division, Bhabha Atomic Research Centre, Mumbai 400085, India
[3]Homi Bhabha National Institute, Anushaktinagar, Mumbai 400094, India
[4]Department of Physics, University of Illinois Chicago, Chicago, Illinois 60607, USA

(Received 5 July 2024; revised 5 November 2024; accepted 13 February 2025; published 26 March 2025)

Most reported negative linear compressibility (NLC) materials exhibit either a small NLC over a large pressure range or a high NLC over a very small pressure range. Here, we report the remarkable discovery of giant NLC in the low-temperature form of CuCN (LT-CuCN) over an unusually large pressure range. High-pressure XRD studies on LT-CuCN observed the NLC of -20.5 TPa^{-1} along the a axis at zero pressure, and the ambient orthorhombic phase remained stable up to 9.8 GPa. Pressure- and temperature-dependent Raman studies identified the phonon vibrations responsible for NLC and negative thermal expansion (NTE).

DOI: 10.1103/PhysRevLett.134.126102

Under hydrostatic compression, most materials usually contract in all crystal directions, showing positive linear compressibility (PLC). However, in rare cases, some materials expand along one or more crystal directions, demonstrating negative linear compressibility (NLC) or negative area compressibility (NAC). NLC is a relatively very weak phenomenon compared to the typical PLC in materials [1,2]. Very few materials have been reported to have strong NLC; most are found in framework structures. The maximum NLC observed till now in cyanides is -76 TPa^{-1}(K_c) in $Ag_3[Co(CN)_6]$ along the c direction and only up to 0.19 GPa of pressure [3], above which it undergoes a structural phase transition [3–5]. Another notable example is the giant NLC of $-42(5)$ TPa^{-1} in Zinc dicyanoaurate $Zn[Au(CN)_2]$ along the c direction but only up to 1.8 GPa of pressure, above which it shows structural transition and persisted NLC of $-6(3)$ TPa^{-1} up to 14.2 GPa of pressure [6–8]. Among other NLC materials with a large range, most have very small NLC values; one notable example is β-MnO_2, which shows an NLC of merely -0.16 TPa^{-1} for a pressure range from 0.3 to 29.3 GPa [9]. Most of the materials discovered either have very weak NLC or have a very short range of pressures. Strong NLC materials show structural instability; hence, observing large NLCs for a large pressure range has been challenging.

Anisotropic thermal expansion exhibited by cyanides has been of interest following reports of NLC and colossal negative thermal expansion (NTE) in $Ag_3Co(CN)_6$ [3–5,10]. Several cyanides such as $Ag_3[Co(CN)_6]$, $KMn[Ag(CN)_2]_3$, $KCd[Ag(CN)_2]_3$, and $Zn[Au(CN)_2]_2$ are reported to show both NLC and NTE, simultaneously [3,4,6–8,11–13]. Interestingly, most of these materials show structural phase transition under high pressure by a maximum of about 3 GPa, above which either they amorphized, decomposed, or transitioned into new structures that cease to show NLC and/or NTE. Here, it is quite evident that observing strong NLC for a large pressure range is difficult. Besides, cyanides are also interesting due to their unusual properties, like pressure-induced amorphization (PIA) and pressure-induced polymerization. NLC is also an attractive mechanical property, with a key application being the development of effectively incompressible optical materials [1,2]. Metal cyanides of the type MCN (M = Au, Ag, and Cu) form linear chain structures and show one-dimensional NTE along the chain direction with overall positive thermal expansion [14]. However, there are no reports of NLC in this family of materials. CuCN crystallizes into orthorhombic or hexagonal phases at ambient conditions depending on the synthesis condition, named low-temperature form as LT-CuCN and high-temperature form as HT-CuCN phases, respectively, which are disordered [15,16]. LT-CuCN crystallizes in an orthorhombic $C222_1$ structure with Z = 4, and HT-CuCN crystallizes in a hexagonal $R3m$ structure with Z = 3. The LT-CuCN phase converts irreversibly to the HT-CuCN phase at 563 K [15,16]. Of all the MCN (M = Cu, Ag, and Au), LT-CuCN has the largest coefficient of NTE along the chain direction. For LT-CuCN, NTE along the a direction is -53.8×10^{-6} K^{-1}, and HT-CuCN is -27.9×10^{-6} K^{-1} in the c direction [14].

Like other cyanides where NTE co-existed with strong NLC, it is expected to have strong NLC in LT-CuCN. Hence, the structural properties of LT-CuCN were investigated using x-ray diffraction (XRD) at high pressures. Interestingly, strong NLC is found in LT-CuCN, which remained in the ambient phase over large pressure range. Further, the vibrational properties of LT-CuCN have been

*Contact author: nilesh@uic.edu
†Contact author: rekhar@barc.gov.in

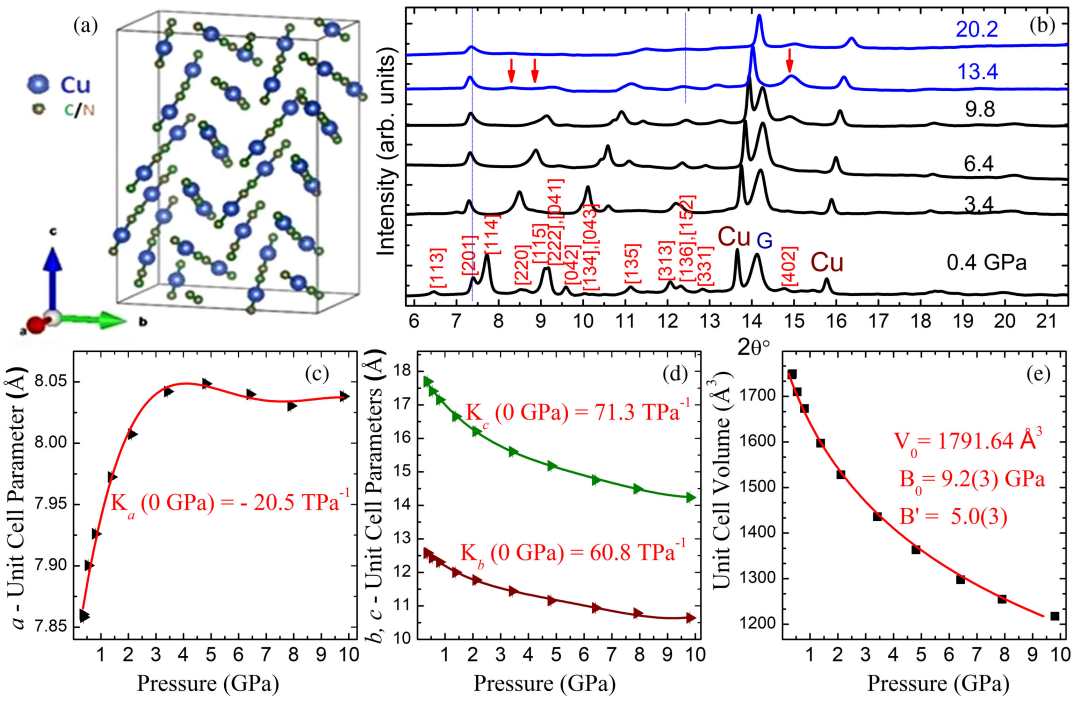

FIG. 1. XRD studies of LT-CuCN at high pressures (a) Crystal structure of the LT-CuCN phase with space group $C222_1$. (b) XRD pattern of LT-CuCN at various high pressures ($\lambda = 0.4957$ Å). Copper peaks are labeled as Cu and used as a pressure marker. Peaks from gasket material are labeled as G. Vertical dotted blue lines are a guide to see the anomalous movement of the peak towards the lower 2θ angles with increasing pressures. The black curve indicates the ambient orthorhombic phase, and the blue curve indicates the new high-pressure phase. (c) Pressure dependence of the a parameter. Black symbols show experimental a parameters. The red curve represents polynomial fit by $a = 7.81(9) + 0.16(2)P - 0.038(7)P^2 + 0.004(1)P^3 - 0.00013(6)P^4$. (d) Variation of b and c parameters with pressure. The green and brown curves represent polynomial fits to the b and c parameter data by $b = 12.83(4) - 0.78(6)P + 0.17(3)P^2 - 0.020(5)P^3 + 0.0009(3)P^4$ and $c = 18.09(3) - 1.29(4)P + 0.24(2)P^2 - 0.024(3)P^3 + 0.0009(2)P^4$ respectively. (e) Variation of unit cell volume with pressure. The red curve represents BM-EOS fitting. Error bars in (c)–(e) are within the symbol size.

investigated by pressure- and temperature-dependent Raman measurement. Raman modes contributing to NTE in LT-CuCN are identified. In addition, Raman spectroscopy has provided valuable information about the mechanism of NLC, the anharmonicity of the modes, and structural stability.

LT-CuCN contains wavelike 1D chains in which two-coordinated Cu are bridged by site-disordered CN [15,16]. Figure 1(a) depicts the crystal structure of LT-CuCN. The structure consists of infinite Cu-CN chains containing five crystallographically distinct Cu atoms with nine CuCN units. Figure 1(b) represents the XRD pattern of LT-CuCN at selected pressures up to 20.2 GPa (See Supplemental Material [17] for experimental details and Fig. S1 for XRD patterns at closer pressure intervals [18–30]). The lattice parameters at several pressures up to 9.8 GPa were refined. The Rietveld refined XRD pattern at (a) 0.4, (b) 0.5, (c) 0.8, (d) 1.4, (e) 2.1, (f) 3.4, (g) 4.8, (h) 6.4, (i) 7.9, and (j) 9.8 GPa pressures are shown in Supplemental Material Fig. S2 [17], and the variation of lattice parameters and unit cell volume of LT-CuCN with pressure is shown in Figs. 1(c)–1(e). The refined atom positions (Cu positions were refined while the C and N positions were kept fixed at the reported position [16]) at all the pressure data are given in Supplemental Material Tables S1–S10 [17].

The high-intensity reflection peak appears at 7.7°, marked as [114], moves towards a higher angle under pressure, indicative of lattice compression. Interestingly, the anomalous shift under high pressure is observed on the reflection peak at 7.3°, marked as [201] crystallographic plane. The variation of interplanar spacing of prominent lattice planes of orthorhombic LT-CuCN is shown in Supplemental Material Fig. S3 and Table S11 [17]. The interplanar separation for [201] plane indicates anomalous behavior compared to other planes, indicating NLC. This expansion may lead to a structural phase transition at higher pressures. Apart from this anomalous shift of the diffraction peak, the XRD pattern remains qualitatively similar up to 9.8 GPa. The XRD data analyzed using Rietveld refinement with ambient $C222_1$ structure up to 9.8 GPa. Around 11.6 GPa, a few new reflection peaks appeared at 8.4° and 14.9°, also marked in Fig. 1(b), which could not be fitted with ambient structure. Also, the major reflection peak observed at 7.7° around 0.4 GPa disappears completely by 18 GPa. This

indicates structural phase transition in LT-CuCN above 9.8 GPa of pressure. Bulk modulus is obtained using third-order Birch-Murnaghan equation of State (BM-EOS); zero pressure bulk modulus of LT-CuCN is estimated to be $B_0 = 9.2(3)$ GPa, see Fig. 1(e). The bulk modulus suggests that the compound LT-CuCN is very soft and in the range of many of the observed NLC cyanides. The variation of lattice parameters of LT-CuCN with pressure are shown in Figs. 1(c) and 1(d). It is very important to note here that the lattice parameters "*b*" and "*c*" showed usual contraction under compression, i.e., positive compressibility. In contrast, lattice parameter "*a*" showed interesting, unusual expansion under pressure, i.e., NLC in its orthorhombic phase. The orthorhombic LT-CuCN remains structurally stable and is NLC up to 9.8 GPa. The zero pressure axial compressibility along *a*, *b*, and *c* are estimated to be −20.5, 60.8, and 71.3 TPa^{-1} (K_a, K_b, K_c), respectively. This linear compressibility along the three directions is estimated using polynomial fits, see Figs. 1(c) and 1(d). The bulk modulus calculated using $[1/(K_a + K_b + K_c)]$ is 8.9 GPa, close to the value obtained by fitting experimental volume data to BM-EOS, see Fig. 1(e). Cairns and Goodwin reviewed the use of linear fitting, polynomial fitting, and empirical model [1,6] to estimate the axial compressibility of NLC materials from the pressure variable lattice parameter experiments. The same empirical model is also used in the program PASCAL [31], from which the compressibility for several systems in the literature are obtained. Our data did not fit well with the linear and the empirical models [1,6]; hence, we used polynomial fit in our studies; see Supplemental Figs. S4(a)–S4(c) [17]. We compared the obtained compressibility value of LT-CuCN with those already discovered NLC cyanides $Ag_3[Co(CN)_6]$, $KMn[Ag(CN)_2]_3$, $KCd[Ag(CN)_2]_3$, $Zn[Au(CN)_2]_2$, and $Eu[Ag(CN)_2]_3 \cdot 3H_2O$. In these cyanides, compressibility values were reported using linear fit or from the empirical model. To make a fair comparison, we fitted their reported pressure-dependent lattice parameters using polynomials and estimated the NLC at zero pressure. The polynomial fitting to their reported data is shown in Figs. S5(a) to S5(f) [17]. The zero pressure compressibility along their NLC directions is compared in Supplemental Material Table S12 [17]. The pressure variation of linear compressibility for these cyanides is calculated and shown in Fig. 2. Interestingly, the magnitude of K_a for LT-CuCN ($K_a(0\ \text{GPa}) = -20.5\ TPa^{-1}$) initially decreases and reaches a minimum value of $-1.8\ TPa^{-1}$ at 4.81 GPa, then shows an increment in K_a under higher pressures to again to a larger value of $-9.4\ TPa^{-1}$ at 9.8 GPa. The mean NLC value for LT-CuCN over 0–9.8 GPa pressure range is estimated to $-10.2\ TPa^{-1}$. These studies prove that LT-CuCN has been discovered to be the first cyanide to have a giant NLC compressibility value for a remarkably large pressure range reported so far in the ambient structure. Interestingly, after the transition, the [201] reflection peak, began to shift towards a higher 2θ angle with compression. Simultaneously, another reflection peak at 12.4° around 11.6 GPa shifted towards lower angles at high pressure, indicating that the NLC still exists in the new phase, see Supplemental Material Fig. S1 [17].

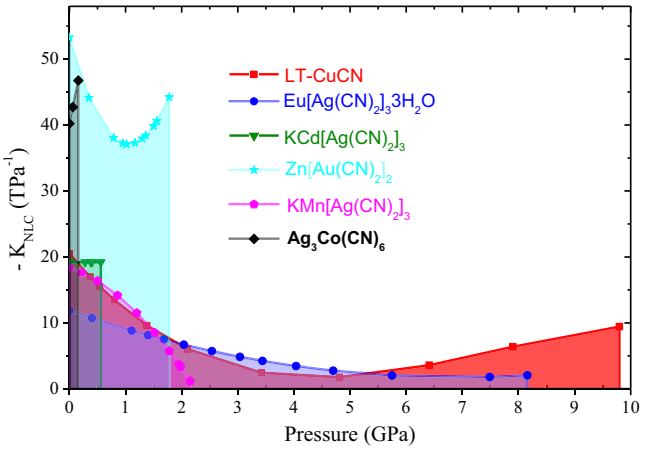

FIG. 2. Pressure variation of Linear compressibility (along the NLC direction) within pressure range of structural stability of their ambient phases of LT-CuCN, $Ag_3[Co(CN)_6]$, $KCd[Ag(CN)_2]_3$, $Zn[Au(CN)_2]_2$, $KMn[Ag(CN)_2]_3$, and $Eu[Ag(CN)_2]_3 \cdot {}_3H_2O$ estimated after fitting polynomials to their lattice parameter data. For polynomial fitting, see Supplemental Material Figs. S5(a)–S5(f) [17].

Observing giant NLC in LT-CuCN up to 9.8 GPa is rare and unique. In the development of effectively incompressible optical materials, NLC will have applications [1,2]. The literature speculates that stronger NLC can be found in framework structures showing very anisotropic NTE, although both can be independent phenomena [1]. It is also interesting to note that the discovered NLC and reported NTE in LT-CuCN are observed along the same *a*-lattice parameter. To our knowledge, only a limited number cyanides, such as $Ag_3[Co(CN)_6]$, $KMn[Ag(CN)_2]_3$, $KCd[Ag(CN)_2]_3$, and $Zn[Au(CN)_2]_2$, were reported to show both NLC and NTE in their ambient phases [3,4,6–8,11–13]. But these materials show structural phase transition at high pressure of 0.19 [3], 1.8 [11,12], 0.5 [13], and 2.8 GPa [6], respectively. Recently $Eu[Ag(CN)_2]_3 \cdot 3H_2O$ is reported to show NLC mean compressibility of $-4.2(1)\ TPa^{-1}$ up to 8.2 GPa [19] which was obtained using a strain tensor. The mean compressibility for $Eu[Ag(CN)_2]_3 \cdot 3H_2O$ using polynomial will be $-6.2\ TPa^{-1}$ for the pressure range 0–8.2 GPa.

In $KMn[Ag(CN)_2]_3$, the NLC was reported to have a mean value of $K_c = -12.0(8)\ TPa^{-1}$ using empirical model fit, which will become $K_c = -11.2\ TPa^{-1}$ (mean value over the experimental data) using polynomial fit. The ambient structure of $KMn[Ag(CN)_2]_3$ changes at 2.8 GPa, followed by PIA at 13.5 GPa. [11,12] In $KCd[Ag(CN)_2]_3$, the NLC was reported to have a mean value of $K_c = -21(2)\ TPa^{-1}$ using linear fit in its first phase followed by

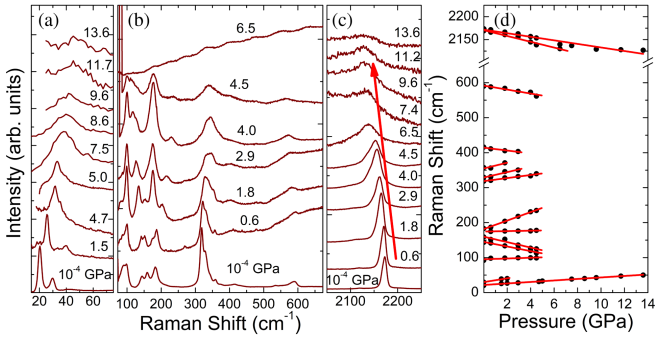

FIG. 3. Raman spectroscopic studies of LT-CuCN at high pressures. (a)–(c) Represent Raman spectra of LT-CuCN at frequency ranges 15-75, 75–675, and 2050–2250 cm^{-1}, respectively. (d) Variation of Raman mode frequencies with pressure. Solid lines indicate a linear fit to the data.

three phase transitions (at 0.5, 2, and 3 GPa) in which all three phases show NLC [13]. In $Zn[Au(CN)_2]_2$, the NLC was observed with a mean value of $K_c = -42(5)$ TPa^{-1} using the empirical model fit, which will be -40.7 TPa^{-1} (mean value over the experimental data) using polynomial fit. The phase transition in $Zn[Au(CN)_2]_2$ appears around 1.8 GPa. [6–8] For $Ag_3[Co(CN)_6]$, the mean value of $K_c = -76$ TPa^{-1} was reported using a linear fit which is also the same as at zero pressure [3]. DFT [32] and DFT + D2 [33] studies on $Ag_3[Co(CN)_6]$ indicated zero pressure NLC value at 0 K of about $K_c = -18.8$ and $K_c = -21$ TPa^{-1}, respectively. A large underestimation of NLC value in theoretical calculation was assigned to the considerable softening of the material on heating [33]. We found that the reported pressure-dependent c-lattice parameter data for $Ag_3[Co(CN)_6]$ (within 0.19 GPa) [3] fit well with the second-order polynomial compared to linear fit, as shown in Supplemental Material Fig. S5(c) [17] with zero pressure $K_c = -40.2$ TPa^{-1}. NLC obtained with polynomial fit is reasonably consistent with theoretically calculated NLC [32,33]. This indicates that proper care should be taken to estimate NLC by ensuring the best fit. The axial compressibility and bulk moduli reported for different cyanides are presented in Table S12 [17] for comparison. We would like to highlight that the mean value of NLC in LT-CuCN is of the same order of magnitude as NLC at zero pressure. However, we believe that the average or mean value does not fully capture the true nature of NLC. Closer data points near the pressure where the NLC is strongest can skew the mean toward higher values. Therefore, specifying the compressibility at zero pressure or at a given pressure is more appropriate than relying on average values. Observation of NLC and structural stability of LT-CuCN in the orthorhombic phase over a large pressure range (up to about 9.8 GPa) makes it a potential candidate for technological applications.

Further, pressure-dependent Raman investigations are also carried out to understand the behavior of phonons in LT-CuCN. Raman spectra of LT-CuCN in three frequency regions at ambient conditions with fifteen different bands are shown in Supplemental Material Fig. S6 [17]. Raman mode frequencies in the bending and stretching region match well with the previously reported Raman spectra of LT-CuCN [16,34]. The Raman bands below 50 cm^{-1} are being reported for the first time here, clearly showing two lattice modes at 20 and 30 cm^{-1}. The modes assignments are taken from the literature. The earlier high-pressure Raman study on LT-CuCN was reported only up to 3.7 GPa [34], which gave limited information. Our interest is to probe the high-pressure vibrational behavior of LT-CuCN in the pressure range in which NLC was discovered. Figures 3(a)–3(c) show the Raman spectra of LT-CuCN at various pressures in the three-frequency range (a) 15-75, (b) 75–675, and (c) 2050–2250 cm^{-1}. Both lattice modes at 20 and 30 cm^{-1} display stiffening with pressure; therefore, they do not contribute to the NTE in LT-CuCN [Figs. 3(a) and 3(d)].

New Raman mode appears around 175 cm^{-1} at 0.6 GPa, showing a continuous increase in intensity with pressure; see Figs. 3(b) and 3(d). It is interesting to note that the modes at 158, 580, and 2170 cm^{-1} assigned to Cu-C-N-Cu bending, Cu-C/N stretching, and the C ≡ N stretching modes, respectively, show unusual softening with pressure as can be seen in Figs. 3(b)–3(d). This softening of the modes reveals abnormal elongation of C ≡ N bonds. An increase in interplanar separation with pressure for [201] plane that is associated with NLC observed in high-pressure XRD can be explained by the softening of the vibrational modes in the Raman spectrum since the CuCN chain is across this plane, and overall chain length could be increasing with pressure.

Mechanisms for observing the NLC property have been classified into four categories viz, (i) NLC as a consequence of ferroelastic phase transition, (ii) NLC driven by correlated polyhedral tilts, (iii) NLC in helical systems, and (iv) NLC due to framework hinging in framework materials [1]. The present NLC material LT-CuCN has an orthorhombic structure containing periodic chains of Cu-C-N-Cu, mostly aligned along the a direction. Under hydrostatic pressure, we observed abnormal elongation of the interplanar spacing of the [201] plane from the XRD investigations and softening of the CN stretching frequency from the Raman investigation. This observation indirectly indicates that the chain length will increase under hydrostatic pressure. From XRD, it was difficult to refine the C and N positions to give a detailed picture of the overall increase in the chain length. Hence, the Cu positions were refined, keeping the C and N positions fixed [16].

Figures 4(a) and 4(b) indicate the arrangement of Cu-CN-Cu chains in the orthorhombic structure when viewed in the ac plane at 0.4 and 4.8 GPa. In Figs. S7(a) to S7(j) [17], the structure of LT-CuCN viewed in the ac plane is given for all the pressure data for better visualization. The structure of LT-CuCN in the ac plane is

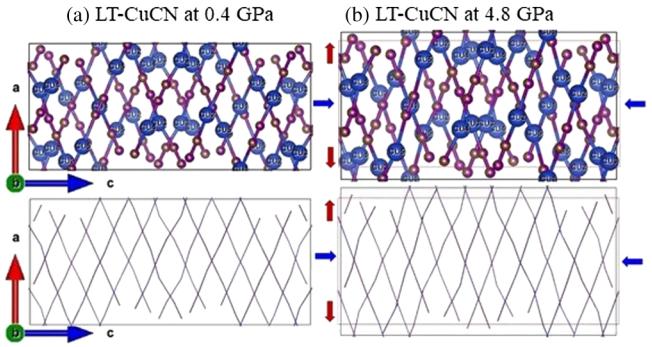

FIG. 4. Structure of LT-CuCN at (a) 0.4 and (b) 4.8 GPa viewed in the *ac* plane. Elongation along the *a* axis under high pressure is observed due to the hinging of the wine rack structure.

a wine rack structure. Hinging of the wine rack network under high pressure is responsible for the unusual elongation of the *a*-lattice parameter. This mechanism explains the NLC observed in the present orthorhombic LT-CuCN. A similar mechanism also has been observed for $Ag_3[Co(CN)_6]$ [3], $KMn[Ag(CN)_2]_3$ [11], $Zn[Au(CN)_2]_2$ [6], and $KCd[Ag(CN)_2]_3$ [13], etc.

Figure 3(d) shows the variation of Raman mode frequencies with pressure, indicating that some modes show softening in addition to the hardening of most other modes. The softening of the C-N stretching mode is marked with an arrow in Fig. 3(c). The variation of Raman mode frequencies of LT-CuCN with pressure fitted linearly and the slopes are given in Table S13 [17]. From Figs. 3(a)–3(c), it is also clear that the intensity of all the Raman modes is reduced. Raman spectra in the middle-frequency region disappeared above 7 GPa. In addition, ultralow frequency and the C-N stretching frequency modes remained visible (although weak in intensity) with almost similar pressure-frequency dependence up to 13.6 GPa, see Figs. 3(a) and 3(c). Above 13.6 GPa, the whole of the Raman spectra disappeared. This confirms that the crystal structure of LT-CuCN is changing, as also observed in high-pressure XRD. Since Raman spectroscopy is a local probe that has detected the transition starting around 7 GPa and completing above 13.6 GPa. However, the Raman modes had no significant broadening before the spectra disappeared. Hence, amorphization is ruled out, which is consistent with XRD results. The complete disappearance of the Raman spectra indicates phase transition at high pressure, and the continuous softening of the $C \equiv N$ stretching mode is a precursor for that. However, when released from 20.2 GPa, the signatures of the ambient LT-CuCN phase were observed in Raman and XRD measurement, indicating the reversible nature of the phase transition (see Figs. S8 and S9 [17]). Further, anharmonicity in LT-CuCN is discussed in the Supplemental Material [17].

In conclusion, high-pressure XRD and Raman spectroscopic investigations were carried out on LT-CuCN up to 20.2 and 13.6 GPa, respectively. The compound LT-CuCN, known for its NTE, is discovered to have large anisotropic compressibility, showing NLC along the *a* axis over a wide pressure range of 0–9.8 GPa due to the hinging of its wine rack structure. Some of the Raman modes in LT-CuCN that show softening under high pressure are identified. Changes observed in Raman spectra above 13.6 GPa are consistent with the XRD pattern above 9.8 GPa, which indicates a structural phase transition.

Acknowledgments—S. K., A. B. G., and R. R. acknowledge DST, India, for the financial support for the work done at the Elettra synchrotron source with Proposal No. 20165031. Dr. Boby Joseph is acknowledged for help at the beamline. The authors thank Dr. S. N. Achary of the Chemistry Division, Bhabha Atomic Research Centre, for providing XRD data of LT-CuCN at ambient conditions. N. P. S. acknowledges support by DOE-SC (DE-SC0020340), DOE-NNSA (DE-NA0004153, CDAC), and NSF (DMR-2119308). N. P. S. acknowledges the support and encouragement of Prof. Russell J. Hemley. VESTA Software is used for Structure visualization.

[1] A. B. Cairns and A. L. Goodwin, Negative linear compressibility, Phys. Chem. Chem. Phys. **17**, 20449 (2015).
[2] R. H. Baughman, S. Stafström, C. Cui, and S. O. Dantas, Materials with negative compressibilities in one or more dimensions, Science **279**, 1522 (1998).
[3] A. L. Goodwin, D. A. Keen, and M. G. Tucker, Large negative linear compressibility of $Ag_3[Co(CN)_6]$, Proc. Natl. Acad. Sci. U.S.A. **105**, 18708 (2008).
[4] L. Wang, C. Wang, H. Luo, and Y. Sun, Correlation between uniaxial negative thermal expansion and negative linear compressibility in $Ag_3[Co(CN)_6]$, J. Phys. Chem. C **121**, 333 (2017).
[5] R. Rao, S. N. Achary, A. K. Tyagi, and T. Sakuntala, Raman spectroscopic study of high-pressure behavior of $Ag_3[Co(CN)_6]$, Phys. Rev. B **84**, 054107 (2011).
[6] A. B. Cairns, J. Catafesta, C. Levelut, J. Rouquette, A. van der Lee, L. Peters, A. L. Thompson, V. Dmitriev, J. Haines, and A. L. Goodwin, Giant negative linear compressibility in zinc dicyanoaurate, Nat. Mater. **12**, 212 (2013).
[7] M. K. Gupta, B. Singh, R. Mittal, M. Zbiri, A. B. Cairns, A. L. Goodwin, H. Schober, and S. L. Chaplot, Anomalous thermal expansion, negative linear compressibility, and high-pressure phase transition in $ZnAu_2(CN)_4$: Neutron inelastic scattering and lattice dynamics studies, Phys. Rev. B **96**, 214303 (2017).
[8] L. Wang, H. Luo, S. Deng, Y. Sun, and C. Wang, Uniaxial negative thermal expansion, negative linear compressibility, and negative Poisson's ratio induced by specific topology in $Zn[Au(CN)_2]_2$, Inorg. Chem. **56**, 15101 (2017).
[9] J. Haines, J. M. Léger, and S. Hoyau, Second-order rutile-type to CaCl2-type phase transition in β-MnO2 at high pressure, J. Phys. Chem. Solids **56**, 965 (1995).
[10] A. L. Goodwin, M. Calleja, M. J. Conterio, M. T. Dove, J. S. O. Evans, D. A. Keen, L. Peters, and M. G. Tucker,

Colossal positive and negative thermal expansion in the framework material $Ag_3[Co(CN)_6]$, Science **319**, 794 (2008).
[11] A. B. Cairns, A. L. Thompson, M. G. Tucker, J. Haines, and A. L. Goodwin, Rational design of materials with extreme negative compressibility: Selective soft-mode frustration in $KMn[Ag(CN)_2]_3$, J. Am. Chem. Soc. **134**, 4454 (2012).
[12] K. Kamali, C. Ravi, T. R. Ravindran, R. M. Sarguna, T. N. Sairam, and G. Kaur, Linear compressibility and thermal expansion of $KMn[Ag(CN)_2]_3$ studied by Raman spectroscopy and first-principles calculations, J. Phys. Chem. C **117**, 25704 (2013).
[13] A. B. Cairns, J. Catafesta, P. Hermet, J. Rouquette, C. Levelut, D. Maurin, A. van der Lee, V. Dmitriev, J. Bantignies, A. L. Goodwin, and J. Haines, Effect of extra-framework cations on negative linear compressibility and high-pressure phase transitions: A study of $KCd[Ag(CN)_2]_3$, J. Phys. Chem. C Nanomater. Interfaces **124**, 6896 (2020).
[14] S. J. Hibble, G. B. Wood, E. J. Bilbé, A. H. Pohl, M. G. Tucker, A. C. Hannon, and A. M. Chippindale, Structures and negative thermal expansion properties of the one-dimensional cyanides, CuCN, AgCN and AuCN, Z. Kristallogr. **225**, 457 (2010).
[15] O. Reckeweg, C. Lind, A. Simon, and J. Salvo, Synthesis, thermal and X-ray investigations of the high-temperature phase of copper(I) cyanide, Z. Naturforsch. B **58**, 155 (2003).
[16] S. J. Hibble, S. G. Eversfield, A. R. Cowley, and A. M. Chippindale, Copper(I) cyanide: A simple compound with a complicated structure and surprising room-temperature reactivity, Angew. Chem., Int. Ed. Engl. **43**, 628 (2004).
[17] See Supplemental Material at http://link.aps.org/supplemental/10.1103/PhysRevLett.134.126102 for experimental details and a discussion about soft modes, structural stability, and anharmonicity. It also includes Figs. S1–S10, Tables S1–S14, and a bibliography containing Refs. [18–30].
[18] H. M. Rietveld, A profile refinement method for nuclear and magnetic structures, J. Appl. Crystallogr. **2**, 65 (1969).
[19] Y. Liu, B. Fu, M. Wu, W. He, D. Liu, F. Liu, L. Wang, H. Liu, K. Wang, and W. Cai, Negative linear compressibility and strong enhancement of emission in $Eu[Ag(CN)_2]_3 \cdot 3H_2O$ under pressure, Phys. Chem. Chem. Phys. **26**, 1722 (2024).
[20] A. P. Roy, S. K. Deb, M. A. Rekha, and A. K. Sinha, Multichannel Raman spectroscopy, Indian J. Pure Appl. Phys. **30**, 724 (1992).
[21] S. Klotz, J.-C. Chervin, P. Munsch, and G. Le Marchand, Hydrostatic limits of 11 pressure transmitting media, J. Phys. D **42**, 075413 (2009).
[22] G. J. Piermarini, S. Block, J. D. Barnett, and R. A. Forman, Calibration of the pressure dependence of the R1 ruby fluorescence line to 195 kbar, J. Appl. Phys. **46**, 2774 (1975).
[23] A. Dewaele, P. Loubeyre, and M. Mezouar, Equations of state of six metals above 94 GPa, Phys. Rev. B **70**, 094112 (2004).
[24] A. P. Hammersley, S. O. Svensson, M. Hanfland, A. N. Fitch, and D. Hausermann, Two-dimensional detector software: From real detector to idealised image or two-theta scan, High Press. Res. **14**, 235 (1996).
[25] A. C. Larson, GSAS, General Structure Analysis System, Report LAUR 86–748, Los Alamos Natonal Laboratory, 1990, pp. 121–124.
[26] G. Venkataraman, Soft modes and structural phase transitions, Bull. Mater. Sci. **1**, 129 (1979).
[27] W. Cochran, Soft modes, a personal perspective, Ferroelectrics **35**, 3 (2011).
[28] G. H. Wolf and R. Jeanloz, Lindemann melting law: Anharmonic correction and test of its validity for minerals, J. Geophys. Res. **89**, 7821 (1984).
[29] A. A. Maradudin and A. E. Fein, Scattering of neutrons by an anharmonic crystal, Phys. Rev. **128**, 2589 (1962).
[30] G. Lucazeau, Effect of pressure and temperature on Raman spectra of solids: Anharmonicity, J. Raman Spectrosc. **34**, 478 (2003).
[31] M. J. Cliffe and A. L. Goodwin, PASCal: A principal axis strain calculator for thermal expansion and compressibility determination, J. Appl. Crystallogr. **45**, 1321 (2012).
[32] P. Hermet, J. Catafesta, J.-L. Bantignies, C. Levelut, D. Maurin, A. B. Cairns, A. L. Goodwin, and J. Haines, Vibrational and thermal properties of $Ag_3[Co(CN)_6]$ from first-principles calculations and infrared spectroscopy, J. Phys. Chem. C **117**, 12848 (2013).
[33] H. Fang, M. T. Dove, and K. Refson, Ag–Ag dispersive interaction and physical properties of $Ag_3[Co(CN)_6]$, Phys. Rev. B **90**, 054302 (2014).
[34] C. Romao, M. M. Barsan, I. S. Butler, and D. F. R. Gilson, A high-pressure micro-Raman spectroscopic study of copper cyanide, CuCN, J. Mater. Sci. **45**, 2518 (2010).